

The Influence of the Technological Parameters on the Ionic Conductivity of Samarium Doped Ceria Thin Films

Mantas SRIUBAS, Giedrius LAUKAITIS*

Physics Department, Kaunas University of Technology, Studentu str. 50, LT-51368 Kaunas, Lithuania

crossref <http://dx.doi.org/10.5755/j01.ms.21.1.5700>

Received 12 November 2013; accepted 27 February 2014

Sm_{0.20}Ce_{0.80}O₂ powder was used for the formation of samarium doped cerium oxide (SDC) thin films using e-beam physical vapour deposition. Surface area of powder was 34.9 m²/g and particle size – 0.3 μm–0.5 μm. Thin films were deposited using physical vapor deposition system on SiO₂ (optical quartz) and Alloy 600 substrates. The deposition rate 0.2 nm/s ÷ 1.6 nm/s and substrate temperature 20 °C ÷ 600 °C were used. Ionic conductivity investigation revealed that the maximum ionic conductivity (1.67 S/m) has the thin film deposited on 300 °C temperature substrate using 0.4 nm/s deposition rate. Minimum ionic conductivity (0.26 S/m) has thin film, which was deposited on 20 °C temperature substrate using 0.8 nm/s deposition rate. Vacancy activation energies vary in 0.87 eV ÷ 0.97 eV range. Furthermore the calculations of crystallite size revealed that crystallite size increases with increasing substrate temperature: from 7.50 nm to 46.23 nm on SiO₂ substrate and from 9.30 nm to 44.62 nm on Alloy 600 substrate. Molar concentration of samarium in initial evaporated material is 19.38 mol % and varies from 11.37 mol % to 21 mol % in formed thin films depending on technological parameters.

Keywords: samarium doped cerium oxide (SDC), e-beam physical vapour deposition, solid oxide fuel cells (SOFC), thin films, ionic conductivity.

1. INTRODUCTION

Wide area of application makes CeO₂ one of the most important oxides among rare earth oxides. This oxide can be used in solid oxide fuel cells (SOFC), gas sensors, UV-blocking materials, smart windows and free-radical scavengers. In addition it can be used as insulator, catalyst material, high refractive index material, anticorrosive coating, etc [1–3].

High interest is due to ceria properties. It has high melting (2477 °C) and boiling (3227 °C) temperatures, calcium fluoride type of structure with space group Fm3m, 12 W/(m·K) thermal conductivity, 165 GPa Young's modulus, ~2 refractive index [4]. Also it is insoluble, has high transparency in the visible-near infrared regions, chemical stability, good adhesion, thermal stability, ~3.6 eV band gap, etc [5].

CeO₂ properties vary under influence of dopants addition, stoichiometry changes, formation methods and formation parameters. For example, pentavalent dopants produce p type conductivity. Vanadium doped ceria (CeVO₄) can be used as counter electrode for Li⁺ ions storage in smart windows [2, 6].

Oxygen ion conductivity in pure ceria is low. It is 5·10⁻⁵ S/cm at 600 °C [7]. If CeO_{2-x} is non-stoichiometric the ionic conductivity increases compared to pure ceria, as non-stoichiometric ceria has more oxygen vacancies. Oxygen vacancies can be produced by adding a particular amount of divalent and trivalent cation dopants also. Generally La₂O₃, Y₂O₃, Sm₂O₃, Gd₂O₃, Na₂O, CaO, SrO are used as dopant material [8].

The most promising materials for O⁻² conductors in intermediate temperatures are Sm₂O₃ and Gd₂O₃ doped

ceria. It exhibits higher ionic conductivity (about 3 times at temperature range of 500 °C ÷ 600 °C) than yttrium stabilized zirconium oxide (YSZ), better chemical, mechanical and thermal compatibility with anode and cathode [9].

Conductivity depends on technological parameters, composition and microstructure of ceria [10]. Changes in processing may change composition and microstructure. Changes in composition and microstructure can affect conductivity. Finding an appropriate relationship between these parameters is very important for the development of high ionic conductivity materials. Intensive research is carried out for this reason.

The aim of this work is to form samarium doped cerium oxide (SDC) thin films using e-beam physical vapour deposition and to investigate the influence of the substrate type and deposition parameters on SDC thin films properties and ionic conductivity.

2. EXPERIMENTAL

Sm_{0.20}Ce_{0.80}O₂ powder was used for the deposition of samarium doped cerium oxide thin films. Surface area of powder was 34.9 m²/g and particle size – 0.3 μm ÷ 0.5 μm. SDC powder was pressed to the pellets with mechanical press. Pressed pellets were annealed at 300 °C temperature.

Thin films (thickness ~1.2 μm) were deposited using e-beam physical vapour deposition system (Kurt J. Lesker EB-PVD 75) on SiO₂ and Alloy 600 substrates. SiO₂ (Süsse GmbH) substrates have 8.36·10⁻⁶ °C⁻¹ thermal expansion coefficient and Alloy 600 (Goodfellow GmbH) have 12.4·10⁻⁶ °C⁻¹ thermal expansion coefficient. The substrates were cleaned in an ultrasonic bath in pure acetone. Cleaned substrates were placed in a vacuum chamber and treated with Ar⁺ ion plasma (10 min) before deposition. The main technological parameters of the thin films deposition were:

*Corresponding author. Tel.: +370-37-300340, fax: +370-37-300302.
E-mail address: gielauk@ktu.lt (G. Laukaitis)

deposition rate of thin film ($0.2 \text{ nm/s} \div 1.6 \text{ nm/s}$), substrate temperature ($20^\circ\text{C} \div 600^\circ\text{C}$) and work pressure ($3 \cdot 10^{-2} \text{ mbar} \div 4.6 \cdot 10^{-3} \text{ mbar}$).

Ionic conductivity of the deposited thin films was investigated using impedance spectrometer (NorECsAS). Measurements were carried out using two-probe method. Frequency range was $0.1 \text{ MHz} \div 1 \text{ MHz}$ and measurement temperature was $200^\circ\text{C} \div 600^\circ\text{C}$.

Pt electrodes were formed on SDC thin films before the electrical measurements. The template was placed on the surface of the thin film and then Pt paste was applied. Later the template was removed and the thin film with Pt paste was annealed at 500°C temperature for 1 hour. Distance between the electrodes was 10 mm and size – $(3 \times 10) \text{ mm}^2$.

Topographic view and roughness measurements of the SDC thin films were carried out with an atomic force microscope “AFM NT-206” using dynamic mode during measurements. Surface roughness (R_q) was calculated using topographic view and “Surface Explorer” software.

Structure of the deposited thin films was investigated by X-ray diffractometer (Bruker D8 Discover). Measurements were carried out in a $20^\circ - 70^\circ$ range using $\text{Cu K}\alpha$ ($\lambda = 0.154059 \text{ nm}$) radiation. Lattice type and crystallite size were estimated by “EVA” and “TOPAS” software using standard Scherrer’s equation [11].

Surface topography photos, cross section photos and elemental composition analysis were carried out with a scanning electron microscope “Hitachi S-3400N” and energy-dispersive X-ray spectroscopy – “Bruker XFlash QUAD 5040”.

3. RESULTS AND DISCUSSION

X-ray diffraction patterns of SDC powder and SDC thin films shows the characteristic peaks corresponding to crystallographic orientations (111), (200), (220), (311), (222) (Fig. 1). The preferential out-of-plane orientation is (111) for the formed thin films. According to XRD data SDC thin films have calcium fluoride type structure with space group $\text{Fm}\bar{3}\text{m}$.

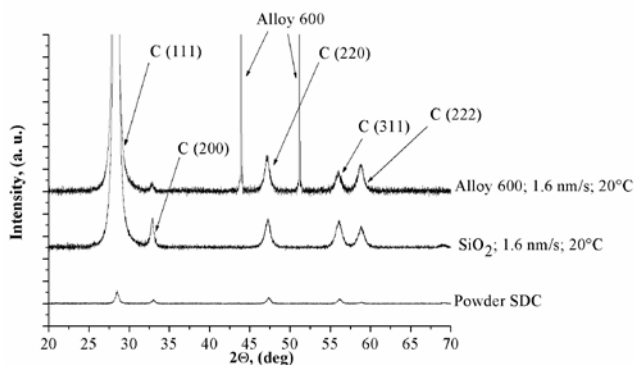


Fig. 1. XRD patterns of SDC powder and thin films deposited on optical quartz (SiO_2) and Alloy 600 substrates using 1.6 nm/s deposition rate at 20°C temperature

Thin films deposited on room temperature (20°C) substrates are nanocrystalline. It does not agree with the results of H. Hong-Hsin [12]. The films formed using e-beam physical vapour deposition were amorphous. According to H. Hong-Hsin, the mobility of the absorbed

species is relatively low, thus preventing their migration to lower energy sites where nucleation could occur [12]. Such disagreement may happen due to the deposition rate difference. Author may use much higher deposition rate than it was in our experiments. It is known that the increasing deposition rate decreases the critical nuclei size. Hence thin films, which were formed using high deposition rate, have small crystallites [13].

Crystallite size calculations revealed that using SiO_2 substrates the crystallite size increases with increasing the substrate temperature (Fig. 2, a). The crystallites of SDC thin films vary from 7.50 nm to 46.23 nm .

The crystallite size changes from 9.30 nm to 44.62 nm for the thin films deposited on Alloy 600 substrates (Fig. 2, b). Crystallites are $9.30 \text{ nm} \div 19.23 \text{ nm}$ using lower temperature (20°C ; 150°C) substrates and $14.05 \text{ nm} \div 44.62 \text{ nm}$ using higher temperature (300°C ; 450°C ; 600°C) substrates. Values of minimum and maximum crystallite size are similar for different type of substrates (Fig. 2). Such dependency of crystallites size and temperature of substrates is related to adatoms energy. Adatoms migration energy is low at low substrate temperature, so the crystallites are small. If the temperature is higher, the adatoms migration energy becomes higher too, therefore the crystallites grow larger [13].

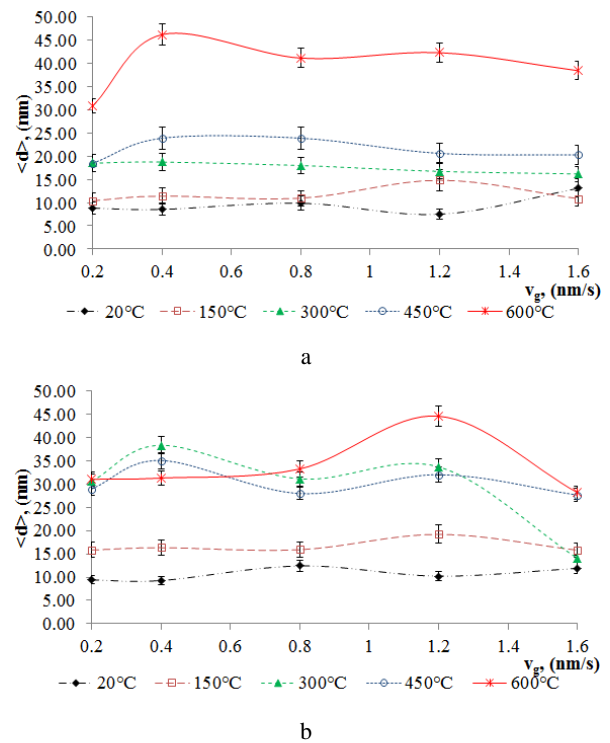


Fig. 2. Crystallite size dependence on the deposition rate: a – optical quartz (SiO_2) substrate; b – Alloy 600 substrate

Samarium molar concentration in SDC powder pellets are $19.38 \text{ mol}\%$ and in deposited SDC thin films are $11.37 \text{ mol}\% \div 21 \text{ mol}\%$ (Fig. 3). Almost all formed thin films have lower dopants concentration, with the exception of the thin film deposited on the 150°C temperature substrate using 1.6 nm/s deposition rate. This SDC thin film has $21 \text{ mol}\%$ concentration of samarium. Four experimental points have similar molar concentrations of the dopant to SDC powder. The difference is within

1 mol %. These thin films were formed using 20 °C, 300 °C temperature substrates and 0.2 nm/s, 0.4 nm/s deposition rates. Such difference may be due to some reasons. Temperature of SDC powder is lower if low deposition rate is used. It means that molecules of SDC powder have lower degree of dissociation than using high deposition rate. Other reason could be the temperature of the substrate. Sticking probability of incident particles is different at different substrate temperatures. Hence SDC thin films will have similar composition to SDC powder if they are deposited using low deposition rate and particular substrate temperature.

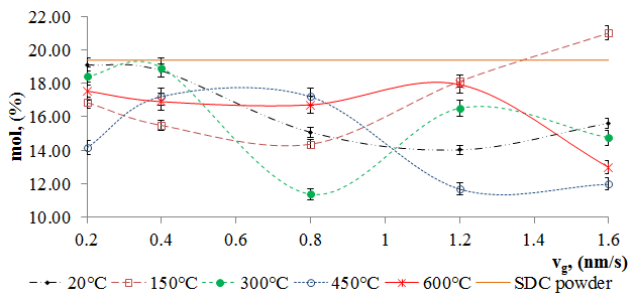


Fig. 3. Dependence of molar concentration of samarium on the deposition rate

SDC thin films grow by the Volmer-Weber growth mechanism [14]. From SEM and AFM it is visible the flat grains growing on the top of each other (Figs. 4–5). They have about 125 nm lengths and about 20 nm heights.

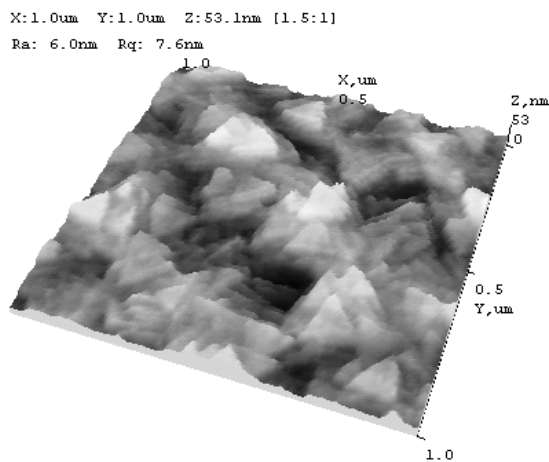


Fig. 4. AFM 3D photo of SDC thin film deposited using 0.8 nm/s deposition rate and 450 °C SiO₂ substrate temperature

Surface of SDC thin films is smooth without cracks and pores (Fig. 5, a–e). In comparison, GDC thin films, which were formed using aerosol deposition method, have cracks and irregular shape grains [15]. SDC thin films have cracks and irregular shape grains if they are deposited using electrodeposition method on steel substrates also [16]. From this point of view, e-beam physical vapour deposition has an advantage over the other methods. Using e-beam physical vapour deposition it is possible to deposit thin films without cracks and with regular shape grains.

Grains may have cupola (Fig. 5, a, c), triangular (Fig. 5, b) or plate shape (Fig. 5, d, e). Thin films deposited on the same temperature substrates using different deposition rate may have different shape and size grains

(Fig. 5, b, c). Similarly it is with the influence of substrate temperature. Thin films deposited on low temperature substrates (20 °C) have small, cupola shape grains and thin films deposited on high temperature substrates (600 °C) have triangular or plate shape grains (Fig. 5, a, d). The same observations are made for SDC thin films deposited at 500 °C temperature on Si (111) substrates. These films have sharp and triangular shape grains [17]. Ytria stabilized zirconia (YSZ) thin films, which were deposited on Ni, Cu-Ni and Hastelloy substrates using e-beam evaporation, have similar structure also [18]. Grain shape and size are different if thin films were deposited on different substrates using the same technological parameters (Fig. 5, b, e). The grains are parallel to the surface using SiO₂ substrate and perpendicular to the surface using Alloy 600 substrate. In comparison with other authors, structure of GDC thin films deposited by aerosol deposition method is different depending on the substrate type, also [15]. According to H. Bae thin films deposited on sapphire substrate have small differences from thin films formed on glass and Pt-Si substrates. However, in our case the difference appears only at particular deposition rates and substrate temperatures. In other words, thin films which were deposited on different type substrates, not necessarily have different surface structure. This implies that the microstructure depends on common influence of substrate type, temperature and deposition rate.

Grain growth of SDC thin films is columnar (Fig. 5, f). The grains grow in I zone and T zone under the structure zone model [18]. On other hand, GDC thin films formed on aluminium plates by RF sputtering method using different O₂/Ar ratios did not show columnar growth [20]. The same results are obtained for GDC thin films formed by spray pyrolysis method on sapphire substrates [21].

The surface roughness of the formed thin films varies from 2.3 nm to 14.1 nm (Fig. 6). It increases with increasing the deposition rate (Fig. 6, a). Such dependence is typical for thin films, which were deposited on the 450 °C, 600 °C temperature substrates. On the contrary, roughness of the thin films does not increase with the increased deposition rate on the 20 °C, 150 °C and 300 °C temperature substrates.

Roughness dependences on the substrate temperature show upward trend (Fig. 6, b). Roughness increases by increasing substrate temperature in all deposition rates. Such dependencies are in agreement with change of crystallite size (Fig. 2). Both crystallite size and roughness of the thin films increase, using higher temperature substrates. However, dependence of the roughness on substrate temperature is nonlinear.

Ionic conductivity of SDC thin films varies from 0.26 S/m to 1.67 S/m at 600 °C temperature (Fig. 7). Ionic conductivity dependencies on the deposition parameters are not linear. One experimental point stands out. SDC thin film deposited on the 300 °C temperature substrate using 0.4 nm/s deposition rate has 1.673 S/m ionic conductivity. This value is similar to one reported in the literature (1.905 S/m) [22]. Ionic conductivity of other thin films varies in the 0.259 S/m–0.869 S/m range.

Ionic conductivity dependencies on the substrate temperature show upward trend (Fig. 7). It is clearly

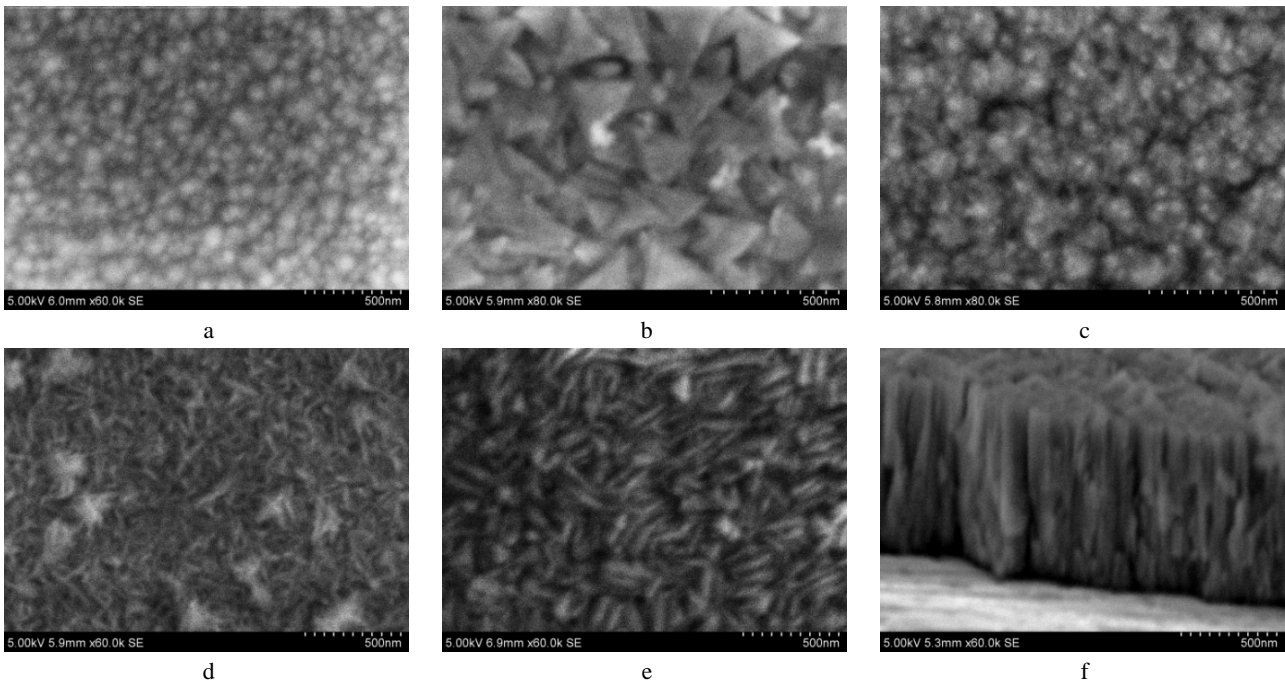


Fig. 5. SEM topographic photos of SDC thin films deposited using: a – 1.6 nm/s – 20 °C, b – 0.8 nm/s – 450 °C, c – 0.2 nm/s – 450 °C, d – 1.6 nm/s – 600 °C deposition rate and substrate temperature on SiO₂ substrate; e – 0.8 nm/s – 450 °C deposition rate and substrate temperature on Alloy 600 substrate. SEM cross sectional view of SDC thin film deposited using: f – 0.2 nm/s – 600 °C deposition rate and substrate temperature on Alloy 600 substrate

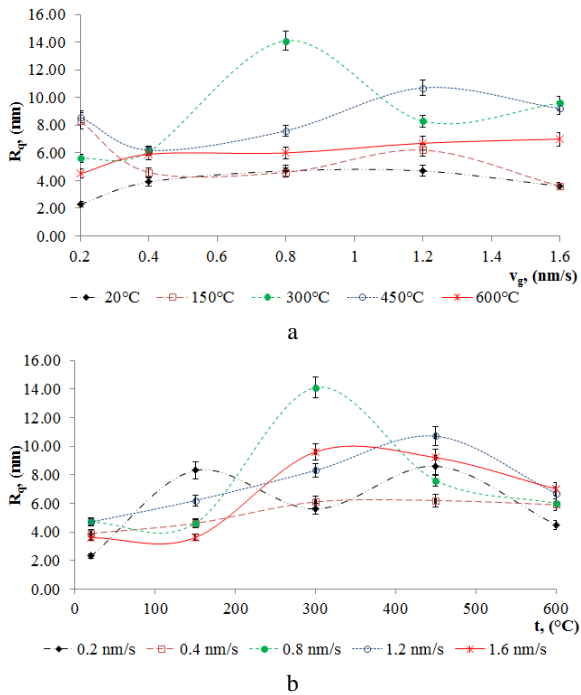


Fig. 6. Roughness dependence of SDC thin filmson: a – SiO₂ substrate temperature; b – deposition rate

Table 1. Oxygen vacancy activation energy values at different deposition parameters

Deposition rate, (nm/s)	Substrate temperature, (°C)				
	20	150	300	450	600
	Oxygen vacancy activation energy, (eV ±0.005)				
0.2	0.912	0.913	0.890	0.927	0.929
0.4	0.891	0.876	0.891	0.889	0.966
0.8	0.936	0.929	0.910	0.885	0.935
1.2	0.936	0.873	0.906	0.875	0.926
1.6	0.888	0.883	0.912	0.911	0.932

visible in minimal values of ionic conductivity. Minimum value of ionic conductivity is 0.259 S/m at 20 °C, 0.299 S/m at 150 °C, 0.536 S/m at 300 °C, 0.575 S/m at 450 °C and 0.661 S/m at 600 °C.

Ionic conductivity values at low deposition temperatures (20 °C ÷ 150 °C) are more sparse than at high deposition temperatures (450 °C ÷ 600 °C) (Fig. 7). The conductivity varies in the 0.832 S/m ÷ 0.257 S/m range using 20 °C temperature substrate and in the 0.661 S/m ÷ 0.603 S/m range using 600 °C substrates. So, it means that the influence of deposition rate decreases with increasing the substrate temperature.

The activation energy of oxygen vacancies was determined using Arrhenius law and the slope of $\log(\sigma)$ vs. $10^3/K$ in Arrhenius plot (Fig. 8) [23]. The activation energies of oxygen vacancies depend on deposition parameters (Fig. 8, Table 1). Dependencies are not linear. The activation energy varies from 0.873 eV to 0.966 eV (Table 1). These energies are higher than given values of doped ceria in the literature (in case of SDC 0.66 eV) [24, 25].

Oxygen vacancy activation energy may depend on the dopant concentration. High dopant concentration may be attributed to the clustering of dopant cations and their associated oxygen vacancies, through which the mobility of oxygen vacancies can be decreased [26, 27]. It means

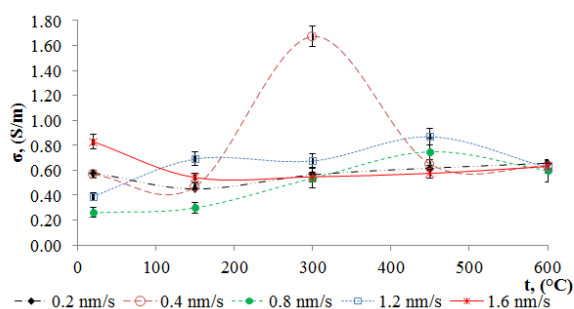


Fig. 7. Ionic conductivity dependencies on SiO₂ substrate temperature

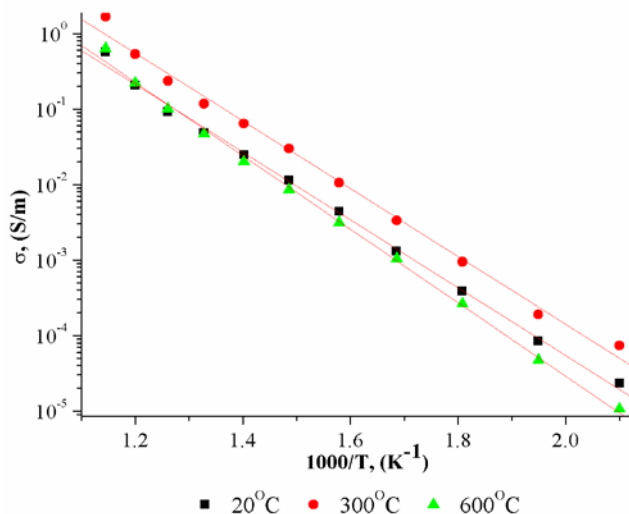


Fig. 8. Arrhenius plots of SDC thin films deposited using 0.4 nm/s deposition rate and 20°C, 300°C and 600°C temperature SiO₂ substrates

that vacancy activation energy increase at high dopant concentrations. Ionic conductivity may depend on oxygen vacancy activation energy. However, the maximum of the ionic conductivity and the minimum of the activation energy are not always associated with the same dopant concentration [28]. Dopant concentration, microstructure and electrical properties of thin films may depend on the technological parameters [10]. So, dopant concentration and microstructure of the thin films may be responsible for the nonlinearity of ionic conductivity (Fig. 7).

4. CONCLUSIONS

SDC thin films were formed using e-beam physical vapour deposition on SiO₂ and Alloy 600 substrates. It was found that the preferred out-of-plane orientation is (111). Further investigation revealed that crystallite size increase with increasing substrate temperature from 7.50 nm to 46.23 nm using SiO₂ substrates and from 9.30 nm to 44.62 nm using Alloy 600 substrates.

Almost all SDC thin films have lower dopant concentration than initial evaporated SDC powder. Samarium molar concentration is 19.38 mol% in initial powder and it changes in the 11.37 mol% ÷ 21 mol% range in thin films. Some of the thin films have similar dopant concentrations to SDC powder. The difference of the concentration is lower than <1 mol% between SDC powder and these SDC thin films. They were formed using

20°C, 300°C temperature substrates and 0.2 nm/s, 0.4 nm/s deposition rates.

SEM photos of SDC thin films show that surface microstructure depends on common influence of substrate type, temperature and deposition rate. Using different deposition parameters, thin films surface have different shape and orientation grains.

Roughness of the thin films varies from 2.3 nm to 14.1 nm. Roughness dependences of substrate temperature show upward trend. It increases increasing substrate temperature for all deposition rates. Such dependencies are in agreement with the change of crystallite size. Both crystallite size and roughness of the thin films increase nonlinearly, with temperature of the substrates.

Activation energies of oxygen vacancies vary in the 0.87 eV ÷ 0.97 eV range. In addition, it is higher than given values of doped ceria in the literature (in case of SDC 0.66 eV) [23, 24]. Activation energy dependencies on deposition parameters are not linear. Dopant concentration and microstructure of thin films may be responsible for nonlinearity of ionic conductivity and oxygen vacancy activation energy.

Ionic conductivity values vary from 0.26 S/m to 1.67 S/m nonlinearly. This is due to common influence of thin films properties and nonlinearities of these properties.

REFERENCES

1. **Bumajdad, A., Eastoe, J., Mathew, A.** Cerium Oxide Nanoparticles Prepared in Self-assembled Systems *Advances in Colloid and Interface Science* 147–148 2009: pp. 56–66.
2. **Krašovec, U. O., Vuk, A. Š., Orel, B.** Comparative Studies of “All Sol-gel” Electrochromic Windows Employing Various Counter-electrodes *Solar Energy Materials and Solar Cells* , 73 (1) 2002: pp. 21–37. [http://dx.doi.org/10.1016/S0927-0248\(01\)00106-4](http://dx.doi.org/10.1016/S0927-0248(01)00106-4)
3. **Rozhkov, V. A., Petrov, A. I.** Antireflective Cerium and Samarium Oxide Coatings for Silicon Photoelectric Devices *Russian Physics Journal* 37 (9) 1994: pp. 815–818.
4. **Mogensen, M., Sammes, N. M., Tompsett, G. A.** Physical, Chemical and Electrochemical Properties of Pure and Doped Ceria *Solid State Ionics* 129 (1–4) 2000: pp. 63–94.
5. **Balakrishnan, G., Sundari, S. T., Kuppasami, P., Mohan, P. Ch., Srinivasan, M. P., Mohandas, E., Ganesan, V., Sastikumar, D.** A Study of Microstructural and Optical Properties of Nanocrystalline Ceria Thin Films Prepared by Pulsed Laser Deposition *Thin Solid Films* 519 (8) 2011: pp. 2520–2526.
6. **Krasovec, U. O., Orel, B., Vuk, A. Š., Bukovec, N., Reisfeld, R.** Structural and Spectroelectrochemical Investigation of Tetragonal CeVO₄ and Ce/V-oxide Sol-gel Derived Ion-storage Films *Solid State Ionics* 118 1999: pp. 195–214. [http://dx.doi.org/10.1016/S0167-2738\(98\)00456-1](http://dx.doi.org/10.1016/S0167-2738(98)00456-1)
7. **Mahato, N., Gupta, A., Balani, K.** Doped Zirconia and Ceria-based Electrolytes for Solid Oxide Fuel Cells: a Review *Nanomaterials and Energy* 1 (1) 2012: pp. 27–45.
8. **Mangalaraja, R. V., Ananthakumar, S., Uma, K., Jimenez, R. M., Uthayakumar, S., Lopez, M., Camurri, C. P.** Synthesis and Characterization of Gd³⁺ and Sm³⁺ Ion Doped Ceria Electrolytes Through an In-situ Sulphated Combustion Technique *Journal of Ceramic Processing Research* 13 (1) 2012: pp. 15–22.

9. **Fu, C. J., Liu, Q. L., Chan, S. H., Ge, X. M., Pasciak, G.** Effects of Transition Metal Oxides on the Densification of Thin-film GDC Electrolyte and on the Performance of Intermediate-temperature SOFC *International Journal of Hydrogen Energy* 35 (20) 2010: pp. 11200–11207. <http://dx.doi.org/10.1016/j.ijhydene.2010.07.049>
10. **Shiqiang, H., Roller, J., Yick, S., Zhang, X., Decès-Petit, C., Xie, Y., Maric, R., Ghosh, D.** A Brief Review of the Ionic Conductivity Enhancement for Selected Oxide Electrolytes *Journal of Power Sources* 172 (2) 2007: pp. 493–502.
11. **Patil, B. B., Pawar, S. H.** Spray Pyrolytic Synthesis of Samarium Doped Ceria ($\text{Ce}_{0.8}\text{Sm}_{0.2}\text{O}_{1.9}$) Films for Solid Oxide Fuel Cell Applications *Applied Surface Science* 253 (11) 2007: pp. 4994–5002.
12. **Hong-Hsin, H., Hung-Peng, Ch., Yu-Tsang, Ch., Ming-Chih, H., Jenn-Shing, W.** Influence of Annealing Temperature on the Grain Growth of Samarium-doped Ceria *Journal of Crystal Growth* 287 (2) 2006: pp. 458–462.
13. **Deniz, D.** Texture Evolution in Metal Nitride (Aluminum Nitride, Titanium Nitride, Hafnium Nitride) Thin Films Prepared by Off-Normal Incidence Reactive Magnetron Sputtering, Proquest. Umi Dissertation Publishing, New York 2011: pp. 16–22.
14. **Oura, K., Lifshits, V. G., Saranin, A. A., Zotov, A. V., Katayama, M.** Surface Science: An Introduction. Springer, New York, 2003: pp. 357–359. http://dx.doi.org/10.1007/978-3-662-05179-5_14
15. **Bae, H., Choi, J., Choi, G. M.** Electrical Conductivity of Gd-doped Ceria Film Fabricated by Aerosol Deposition Method *Solid State Ionics* 236 2013: pp. 16–21.
16. **Lair, V., Živkovič, L. S., Lupan, O., Ringuède, A.** Synthesis and Characterization of Electrodeposited Samaria and Samaria-doped Ceria Thin Films *Electrochimica Acta* 56 (12) 2011: pp. 4638–4644.
17. **Hartmanova, M., Jergel, M., Mansilla, C., Holgado, J. P., Zemek, J., Jurek, K., Kundracik, F.** Structural Characteristics and Morphology of $\text{Sm}_x\text{Ce}_{1-x}\text{O}_{2-x/2}$ Thin Films *Applied Surface Science* 255 (22) 2009: pp. 9085–9091. <http://dx.doi.org/10.1016/j.apsusc.2009.06.108>
18. **Yang, J., Gong, S. K., Liu, H. Z., Gu, H. W.** Texture and Surface Morphology of Yttria-stabilized Zirconia Buffer Layer on Ni-based Tapes by Electron Beam Evaporation *Physica C: Superconductivity* 386 2003: pp. 337–341. [http://dx.doi.org/10.1016/S0921-4534\(02\)02155-X](http://dx.doi.org/10.1016/S0921-4534(02)02155-X)
19. **Barna, P. B., Adamik, M.** Fundamental Structure Forming Phenomena of Polycrystalline Films and the Structure Zone Models *Thin Solid Films* 317 (1–2) 1998: pp. 27–33.
20. **Kuo, Y. L., Chen, Y. S., Lee, C.** Growth of 20 mol % Gd-doped Ceria Thin Films by RF Reactive Sputtering: The O_2/Ar Flow Ratio Effect *Journal of the European Ceramic Society* 31 (16) 2011: pp. 3127–3135. <http://dx.doi.org/10.1016/j.jeurceramsoc.2011.05.002>
21. **Bieberle-Hütter, A., Reinhard, P., Rupp, J. L. M., Gauckler, L. J.** The Impact of Etching During Microfabrication on the Microstructure and the Electrical Conductivity of Gadolinia-doped Ceria Thin Films *Journal of Power Sources* 196 (15) 2011: pp. 6070–6078.
22. **Sanghavi, R., Devanathan, R., Nandasiri, M. I., Kuchibhatla, S., Kovarik, L., Thevuthasan, S., Prasad, S.** Integrated Experimental and Modeling Study of the Ionic Conductivity of Samaria-doped Ceria Thin Films *Solid State Ionics* 204–205 2011: pp. 13–19.
23. **Laidler, K. J.** The Development of the Arrhenius Equation *Journal of Chemical Education* 61 (6) 1984: p. 498.
24. **Andersson, D. A., Simak, S. I., Skorodumova, N. V., Abrikosov, I. A., Johansson, B.** Optimization of Ionic Conductivity in Doped Ceria *Proceedings of the National Academy of Sciences of the United States of America* 103 (10) 2006: pp. 3518–3521.
25. **Shahriar, A.** Optimization of Ionic Conductivity in Doped Ceria Using Density Functional Theory and Kinetic Lattice Monte Carlo. Arizona State University, Arizona, 2011.
26. **Ou, D. R., Mori, T., Ye, F., Takahashi, M., Zou, J., Drennan, J.** Microstructures and Electrolytic Properties of Yttrium-doped Ceria Electrolytes: Dopant Concentration and Grain Size Dependences *Acta Materialia* 54 (14) 2006: pp. 3737–3746. <http://dx.doi.org/10.1016/j.actamat.2006.04.003>
27. **Ye, F., Mori, T., Ou, D. R., Takahashi, M., Zou, J., Drennan, J.** Ionic Conductivities and Microstructures of Ytterbium-doped Ceria *Journal of The Electrochemical Society* 154 (2) 2007: pp. B180–B185.
28. **Inaba, H., Tagawa, H.** Ceria-based Solid Electrolytes *Solid State Ionics* 83 (1–2) 1996: pp. 1–16. [http://dx.doi.org/10.1016/0167-2738\(95\)00229-4](http://dx.doi.org/10.1016/0167-2738(95)00229-4)